

## REDUCING ARTIFACTS IMPACT ON IVUS AUTOMATIC SEGMENTATION VIA INPAINTING

Hugo Manterola<sup>a,b</sup>, Lucas Lo Vercio<sup>a,b</sup> and Mariana del Fresno<sup>a,c</sup>

<sup>a</sup>PLADEMA, Universidad Nacional del Centro, Tandil, Argentina, <http://www.pladema.net>

<sup>b</sup>Consejo Nacional de Investigaciones Científicas y Técnicas (CONICET)

<sup>c</sup>Comisión de Investigaciones Científicas de la Prov. de Buenos Aires (CIC-PBA)

**Keywords:** Arterial wall, Inpainting, IVUS, Segmentation.

**Abstract.** In this work we present a novel approach that uses digital inpainting to preprocess intravascular ultrasound (IVUS) images to reduce the impact of undesired features. Then, we automatically segment the arterial wall with active contour models. IVUS is a catheter-based medical imaging technique that produces cross-sectional images of blood vessels. Segmentation of vessel wall is particularly useful to study many coronary artery diseases, such as atherosclerosis. Being IVUS a good technology to analyse the anatomy of the arterial wall, the modality may present several artifacts, such as shadows or catheter ring-down, that may difficult further processing. To deal with these artifacts, in this paper we consider an exemplar-oriented inpainting algorithm that replaces the corrupted information by using the unaltered neighbourhood. To determine the impact of this preprocessing step, segmentation results over inpainted and non-inpainted IVUS are presented. The images are compared with manually outlined contours, showing that the inpainting method promotes continuity of the arterial wall and improves the segmentation performance.

## 1 INTRODUCTION

Intravascular ultrasound (IVUS) is a medical imaging technique for vascular diagnosis. It is based in a catheterism with an ultrasound transducer which captures axial images of the vessels. The capture is performed during the mechanical pullback of the transducer at a very slow constant speed (between 0.5mm to 1mm per second). IVUS technology provides high resolution images with speckle noise, typical of ultrasound images ([Abbott and Thurstone, 1979](#); [Loizou and Pattichis, 2008](#)).

IVUS is a study that allows studying the three layers of the arterial wall. Unlike angiography, it provides not only information about the lumen but also about the tissues of the arterial wall and atherosclerotic plaque. Regarding this, IVUS is a good complementary study to angiography. The first arterial tunica, known as intima, is in contact with the arterial lumen, where the blood flows. It is composed by elastic fibers which have high echogenicity. The second layer or media tunica, envelops the intima. It is constituted by muscular cells, and it has lower echogenicity than the intima. Finally, the adventitia is composed by connective tissue and elastic fibers, and it is more echogenic than the intima and media.

Since the 1990s, intima - media thickness (IMT) has been the standard measure to evaluate the progression of atherosclerotic cardiovascular disease. In order to automatically compute this indicator it is necessary to have a robust segmentation algorithm of the vessel wall. IVUS provide valuable anatomical information in that sense. However, due to the high noise level of the ultrasound images and the presence of artifacts, the vessel wall segmentation is not a trivial task and overcoming the artifacts becomes a challenge ([Molinari et al., 2010](#)). In particular, the segmentation complexity in IVUS images is given by echographic reflexions, probe artifacts and atherosclerotic plaque ([Balocco et al., 2014](#)). Consequently, the detection and processing of such artifacts allow the segmentation algorithm to avoid inaccurate edge detection due to partial occlusion of the vessels.

In this context, we present a method to preprocess IVUS images that aims to reduce the impact of artifacts in further vessel wall segmentation. The method is called inpainting and consists in modify and fill corrupted or missing data with existing information in the image. Two different sources of IVUS images provided by [Balocco et al. \(2014\)](#) are used. On the one hand, a set was acquired using Boston Scientific iLab IVUS equipped with a 40 MHz catheter Atlantis SR (Set A). On the other hand, a set was acquired using Volcano Corporation Si5 equipped with a 20 MHz Eagle Eye monorail catheter (Set B). Section 2 presents the common obstacles that affects automatic or semi automatic layers segmentation. Section 3 shows the inpainting method. Furthermore, a media-adventitia segmentation technique is presented in Section 4 which is used in Section 5 to show the positive effects of inpainting method for vessel wall segmentation. Finally, in Section 6, we analyse the obtained results and present some final remarks about the viability of the method.

## 2 OBSTACLES IN IVUS SEGMENTATION

Besides speckle noise, vascular ultrasound images are often degraded by different kind of artifacts which affect image quality. These artifacts are generated by several sources such as the catheter itself or other endoluminal devices (stents), plaques, defects in the acquisition system or in the operator manipulation, among others. All this negative effects are frequently found, sometimes combined, in the IVUS images and make the processing a difficult task. In addition, bifurcations and side vessels may interfere the automatic segmentation. In this section we describe the most frequent difficulties when segmenting lumen-intima and media-adventitia

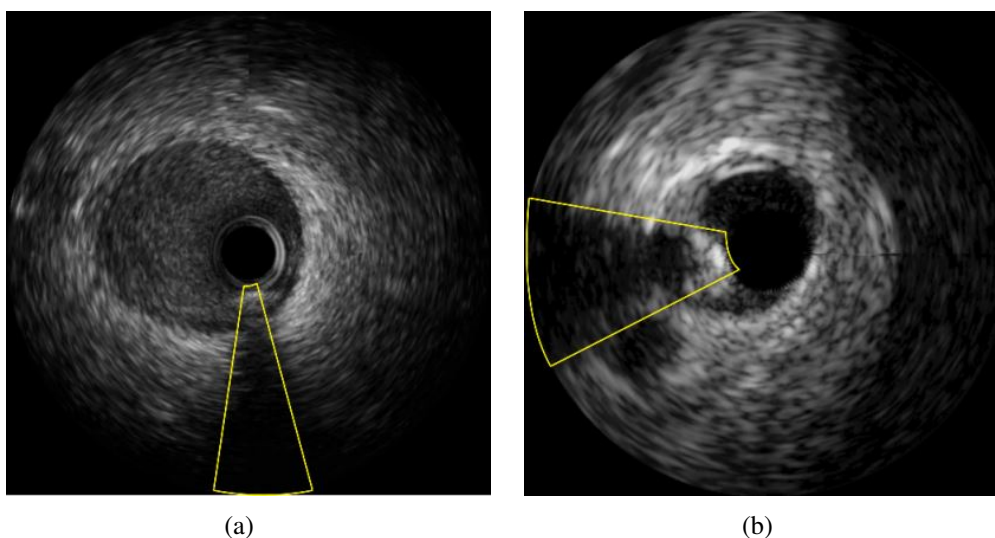


Figure 1: Shadow artifact - marked in solid yellow line (a) Boston Scientific Imaging (b) Volcano Corporation Imaging

interfaces.

## 2.1 Shadow artifact

Shadows in this images are produced when the ultrasound beam can not penetrate an object. As the information behind the occlusion can not be retrieved, the ultrasound system displays a black region. As a consequence a *shadow effect* is observed in the image. Even when this effect can help detecting structures or foreign bodies (e.g. stones in a gallbladder), when it comes to vessel layers segmentation it interferes with the detection of the interfaces between them.

There are different causes of this artifact in the IVUS images. For example, in the case of rotational transducers, there are certain positions where the guidewire of the device obstructs the beam signal, resulting in misleading dark regions. This situation is called *guidewire artifact* (Katouzian et al., 2012). Vessel structures can produce shadows as well. For instance, a plaque with a calcium build-up also produces a shadow due to its high echogenicity. Because of the most of the signal is reflected, the calcification appears as a highly bright region with a much darker region next to it (Taki et al., 2008). The Figure 1 presents examples of shadow artifacts.

## 2.2 Side vessel

In some regions the ultrasound beam penetrates beyond the tissues of the wall that surround the catheter and traces of the adjacent vessels are found. The most discernible of this traces is the lumen which is shown as a low intensity region due to its low echogenicity (Figure 2). This dark region that appears where high intensities are expected (corresponding to the adventitia) is a challenge to segmentation algorithms.

## 2.3 White dots

Horizontal and vertical white dots are used as a ruler by the specialists while viewing an IVUS study (Figure 3). These characteristics are saved over the image and are persisted, for example, in the DICOM files and distributed data sets. These artifacts difficult many segmentation algorithms, like active contours (Balocco et al., 2014).

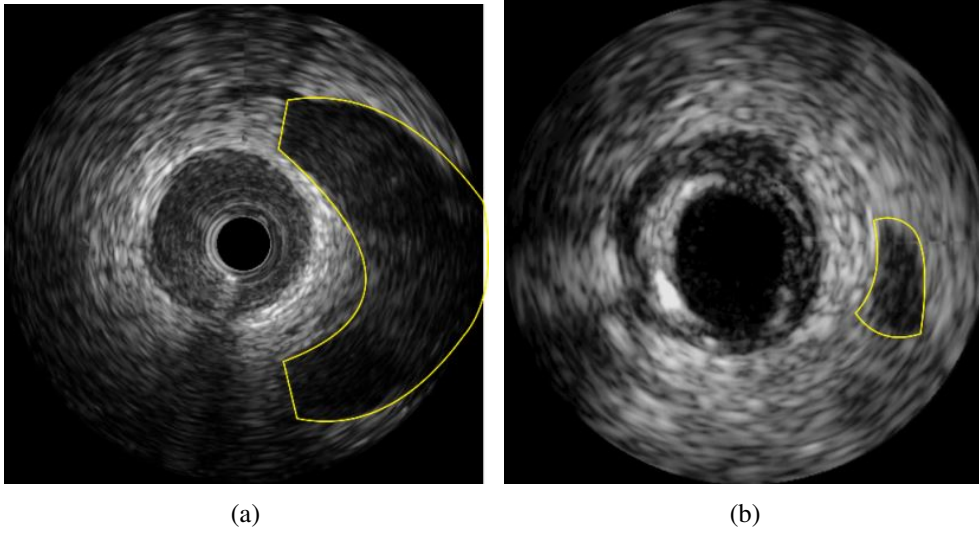


Figure 2: Side Vessel - marked in solid yellow line (a) Boston Scientific Imaging (b) Volcano Corporation Imaging

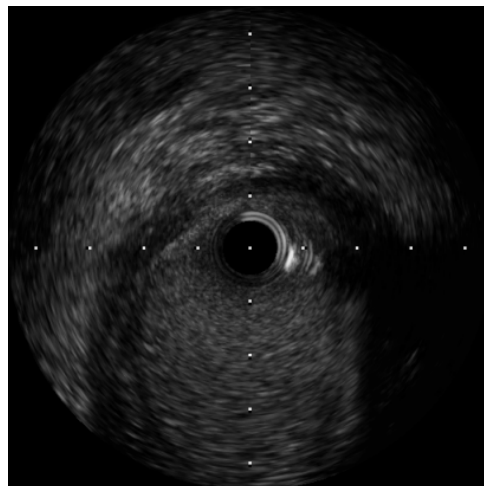


Figure 3: White dots artifact

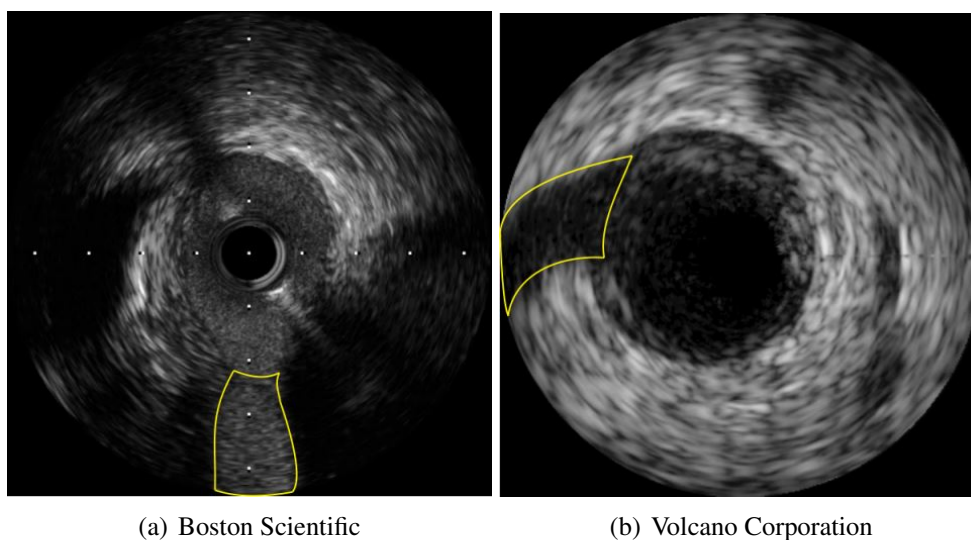


Figure 4: Bifurcation - marked in solid yellow line (Boston Scientific Imaging)

## 2.4 Bifurcations

A bifurcation is a section where the artery diverges into two branches: a main vessel and a lateral vessel with a lower diameter. In hemodynamics, this artifact plays a very important role because the turbulent flow at this point stimulates the plaque evolution (Alberti et al., 2012). In IVUS images, this side branch is shown as a discontinuity of the arterial wall (Figure 4). The ambiguous definition of the vessel in presence of a bifurcation may cause substantial differences between automatic and manual segmentations.

## 3 INPAINTING

### 3.1 Background

Image inpainting was firstly introduced by (Bertalmio et al., 2000). Its purpose is to modify an image and fill the corrupted or missing regions with existing information from surrounding area in a visually plausible way. Since that first approach, a wide variety of related algorithms emerged. In general, any of this techniques need to cope with two main problems when applying inpainting: completing the structure and completing the texture. In the literature, conventional schemes proposed for image inpainting can be divided into two categories: texture-oriented (Efros and Leung, 1999) and structure-oriented (Bornard et al., 2002). On the one hand, the texture-oriented scheme generates the target region with available sample textures from its surroundings. This approach is specifically useful for the images with large texture areas. On the other hand, the structure-oriented scheme obtains the missing regions via data fusion techniques, such as the bilinear interpolation. As shown in (Bornard et al., 2002), the linear structures (i.e., edges or object boundaries) can be preserved and propagated to the target regions. However, since most images are not composed of pure texture or pure structure, better results are expected for those taking advantages of both schemes. Taking this into account, an exemplar-based inpainting technique was adapted to medical imaging (Manterola and del Fresno, 2013). In this proposal, the visible parts of the image (i.e. the non-corrupted sectors) serve as a source set of examples to infer the target regions. Additionally, the filling order is decided by a predefined priority function to ensure that the linear structures will propagate before

texture filling to preserve the connectivity of objects boundaries. Therefore, it is more likely that these structures are preserved and, at the same time, the texture is correctly replicated.

### 3.2 The algorithm

The core of the algorithm is a isophote-driven process. As showed in Figure 5(a),  $R$  is the target region to be filled and  $\delta R$  is its contour. It is expected that this boundary evolves inward as the algorithm proceeds. This is the reason it is called the "fill front". Furthermore,  $I - R$ , that remains fixed throughout all the execution, is the *source region* from which the candidates patches are taken. Let us focus on a single iteration to show how the different components interact and how the exemplar-based synthesis is addressed. Assume that the square  $\Psi_p$  centered in the point  $p$ , in Figure 5(b) is to be replaced. The exemplar that best matches the missing patch is taken from the source region, chosen amongst the candidates  $\Psi_q$  and  $\Psi_{q'}$ , as they lie on the continuation of the same image edge (see Figure 5(c)). The strategy to pick this best candidate will be explained later (for further details, see (Manterola and del Fresno, 2013)). Once this process is finished, the chosen patch  $\Psi_q$  is copied over  $\Psi_p$  (see Figure 5(d)) and the algorithm continues until  $R$  is empty.

Let us now analyse in a general way the region filling algorithm. The only parameter that needs to be provided by the user is the region  $R$  to be replaced. From this region is straightforward to deduce the source region  $I - R$ . Once all this is determined, the algorithm proceeds automatically.

Each pixel of the image has two associated values: the *confidence* which reflects how sure we are about the pixel value and its correspondent *colour* which is empty if it is still unfilled. Moreover, each patch along the frontier  $\delta R$  has a *priority* value that is updated in every iteration and determines the patch which is the best candidate to be filled. Afterward, the algorithm iterates over three steps until every pixel has been filled:

**1 - Compute exemplar priorities.** The *priority* value assigned to each patch in  $\delta R$  determines which one is going to be filled. The patches with the highest priorities are those who are on the continuation of strong edges or that are surrounded by pixels with high *confidence* values. For a patch  $\Psi_p$  centered at the point  $p \in \delta R$ , a priority  $Pr(p)$  is defined as  $P(p) = C(p) * S(p)$  where  $C(p)$  is the *confidence* term and  $S(p)$  is the *strength* term. As can be observed in Figure 5(b), the confidence and the strength can be defined as:

$$C(p) = \frac{\sum_{q \in \Psi_p \cap (I-R)} C(q)}{|\nabla I_p|^\perp}, \quad S(p) = \frac{|\nabla I_p^\perp| \cdot n_p}{\alpha}, \quad (1)$$

where  $|\Psi_p|$  is the area of  $\Psi_p$ ,  $\alpha$  is a normalization factor,  $n_p$  is a unit vector orthogonal to the front  $\delta R$  in the point  $p$  and  $\perp$  denotes the orthogonal operator. The priority  $P(p)$  is computed for every border patch, with distinct patches for each pixel on the boundary of the target region. During initialization, the function  $C(p)$  is set to  $C(p) = 0 \forall p \in R$ , and  $C(p) = 1 \forall p \in I - R$ . The confidence term  $C(p)$  may be thought of as a measure of the amount of reliable information surrounding the pixel  $p$ .

**2 - Propagate texture and structure information.** Once all priorities on the  $\delta R$  have been computed, the patch  $\Psi_p$  with highest priority is found. It is then filled with the patch having the least sum of squared differences. Having found the source exemplar  $\Psi_q$ , the value of each pixel of  $\Psi_p$  is copied from its corresponding position inside  $\Psi_q$ . This achieve the propagation of both structure and texture information from the source  $I - R$  to the target region  $R$ , one patch per iteration.

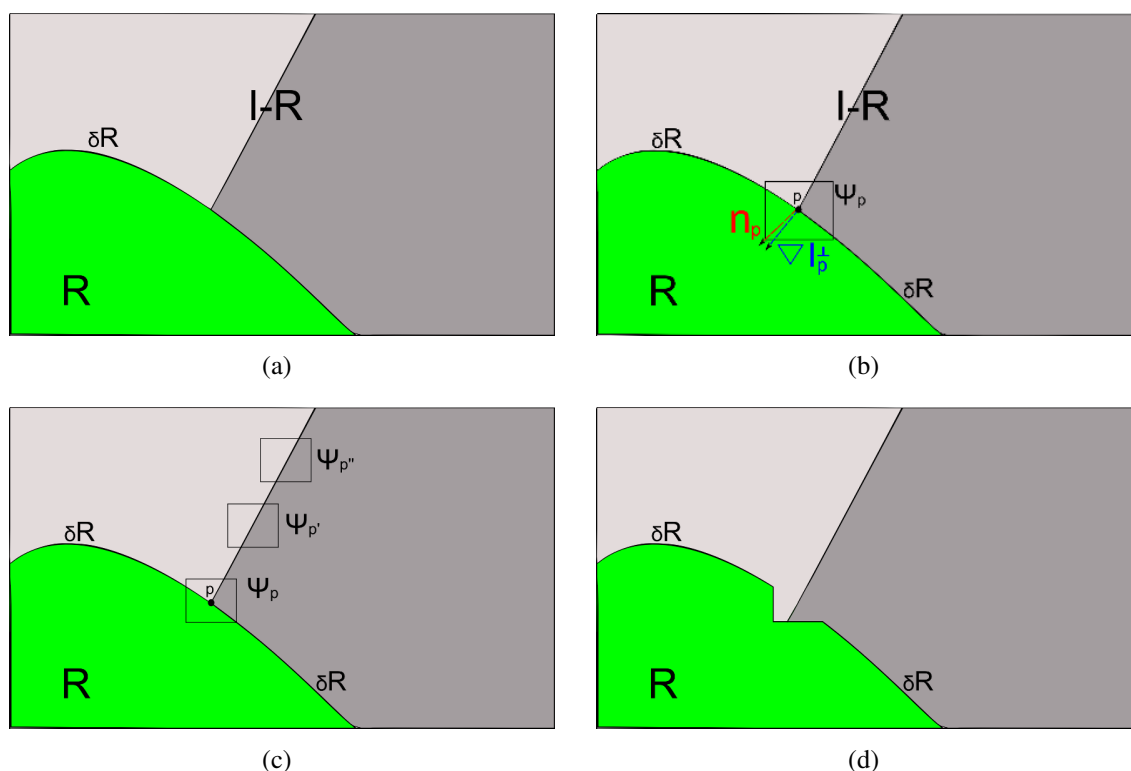


Figure 5: (a) Objective Region  $R$  and source region  $I - R$  (b) Filling order parameters. (c) Candidate patches  $\Psi_{p'}$  and  $\Psi_{p''}$ . (d) Patch restored.

**3 - Update confidence values.** After the patch  $\Psi_p$  has been filled with new pixel values, the confidence  $C(p)$  is updated.

#### 4 MEDIA-ADVENTITIA SEGMENTATION

The segmentation algorithm, based in [Lo Vercio et al. \(2013\)](#), consists of two steps: first, an approximation of the arterial wall is performed using texture analysis ([Haralick et al., 1973](#)) and active contours or *snakes* ([Kass et al., 1988](#); [McInerney and Terzopoulos, 2000](#)); second, a modified version of the snake is used to detect the media-adventitia interface considering an anisotropically diffused image ([Perona and Malik, 1990](#)).

Active contours are widely used for segmenting medical images ([McInerney and Terzopoulos, 1996](#)). Furthermore, they provide an extensible framework to detect objects with unclear boundaries in noisy images. The model consists in a parametric closed curve  $X(u, v) = (x(u, v), y(u, v))$  which is deformed by the action of internal forces (associated with the curve  $X$ ) and external forces (associated with the image  $I$ ). The deformation process stops when the curve no longer changes with further iterations.

The evolution of each node of the curve  $X$  follows the first-order ordinary differential equation of motion:

$$\gamma_i \dot{X}_i + a\alpha_i + b\beta_i = \rho_i + f_i \quad (2)$$

where  $\dot{X}_i$  is the velocity of the node  $X_i$ ,  $\alpha_i$  and  $\beta_i$  are the stretching (Equation 3) and the bending force (Equation 4) at  $X_i$ , respectively. The parameter  $a$  controls the stretching deformation

while  $b$  controls the bending deformation,

$$\alpha_i = (X_i - X_{i-1}) + (X_i - X_{i+1}) \quad (3)$$

$$\beta_i = (\alpha_i - \alpha_{i-1}) + (\alpha_i - \alpha_{i+1}). \quad (4)$$

The external forces are the inflation  $\rho_i$  and the edge attraction  $f_i$ .  $\rho_i$  is a binary function which determines if the curve goes forward or backward in the normal direction  $n_i$ .  $f_i$  is a force associated with the gradient (edges) of the image  $I$ . The parameters  $q$  and  $p$  control the impact of the external forces in the curve evolution.

The Euler method is applied to Equation 2 to update the positions of the node  $X_i$  from time  $t$  to  $t + \Delta t$  according to

$$X_i^{t+\Delta t} = X_i^t - \frac{\Delta t}{\gamma} (a\alpha_i^t + b\beta_i^t - q\rho_i^t - pf_i^t). \quad (5)$$

The Equation 5 iteratively proceeds until the displacement of every node does not exceeds a given error tolerance. The method ensures convergence when the initial contour is placed close enough to the object boundary.

Active contours present a challenge when applied to IVUS segmentation because of the high noise that obstructs the evolution of a curve from the catheter to media-adventitia interface. To overcome this issue, a two-step segmentation is proposed: first, a contour close to the arterial wall is obtained. Second, the media-adventitia segmentation is performed.

#### 4.1 Initial approximation

The lumen has lower intensities than media and adventitia, but it suffers from speckle noise. This effect is visible as bright and dark spots (Loizou and Pattichis, 2008). A texture-based filter is performed to reduce the impact of the noise in the external forces of the curve. This filter uses grey level co-occurrence matrices (GLCM). The GLCM contains the probability of co-occurrence of two grey intensities in a particular or multiple directions (Haralick et al., 1973). In the present work, a GLCM is computed over a square region of radius  $r$  centred in the pixel  $I(x, y)$ . Being  $N$  the possible grey-tone in the image (typically 256), each pixel of the image is transformed into:

$$I^*(x, y) = \sum_{i=0}^{N-1} \left( \sum_{j=0}^{N-1} (i^2 + j^2) P(i, j) \right) \quad (6)$$

where  $P(i, j)$  is the probability of occurrence of the intensities  $i$  and  $j$  in the selected directions obtained from the GLCM.

Then, a region-growing is performed using the textured image  $I^*$ . The method incorporates to the region  $R$  the pixels with lower  $I^*(x, y)$  than a tolerance  $T$  starting from an initial set of points, known as seeds. In this case, the seeds are automatically placed around the circumference of the catheter to avoid the interference of the *ring-down* artifact (Katouzian et al., 2012) and the sections where the catheter is touching the arterial wall (Balocco et al., 2014). The region-growing can stop near intima if it has a high contrast with the lumen, or can stop near adventitia if intima and media present low contrast with each other.

The snake method is used to obtain a smoothed border of  $R$ . As in the previous seed placing, the initial curve is a circumference placed around the catheter. The external forces of the snake

are defined as

$$\rho_i = \begin{cases} n_i & \text{if } X_i \in R \\ -n_i & \text{if } X_i \notin R \end{cases} \quad (7)$$

$$f_i = \nabla I_i^* \quad (8)$$

## 4.2 Final segmentation

Computed a curve close to the arterial wall, a precise segmentation of media-adventitia interface can be performed. The original image  $I$  is filtered using anisotropic diffusion which homogenizes noisy regions and enhance its contours (Perona and Malik, 1990). In this step, the diffused image  $I'$  guides the external forces.

On the one hand, as the adventitia presents higher intensities than the media and lumen, positive gradient in the outgoing radial direction is expected. On the other hand, low or negative gradient values arise beyond the adventitia because the signal maintains high values or is attenuated by the distance from the transducer. Therefore, the inflation force  $\rho$  is defined as

$$\rho_i = F_i n_i \quad (9)$$

where  $F = \nabla I'$ . To generate a more precise segmentation of the media-adventitia interface, the curve is adjusted to the maximum gradient change. Therefore, the external force  $f$  is given by

$$f = \nabla F \quad (10)$$

## 5 RESULTS

The segmentation algorithm presented in Section 4 was used for segmenting IVUS images before and after application of inpainting in the presented obstacles. The tests were performed using two sets of IVUS images from different commercial instrumental commonly used in clinical practice. The obstacles and reference segmentations were marked by trained observers.

Figure 6 shows the application of the inpainting in a particular case of an IVUS image corresponding to Set A. These images usually have at least two features: the shadow artifact and the presence of dots (which are stored over the image). Furthermore, the selected image has a large side vessel. It can be observed in Figure 6(b) that the inpainting process managed to erase the white dots. Figure 6(c) shows the segmentation of the original image, in which the active contour is misguided because of the artifacts. Finally, Figure 6(d) shows the segmentation over the inpainted image where the segmentation is not affected by the presence of white dots and shadow artifact.

Figure 7 depicts the application of inpainting for an IVUS image corresponding to Set B. In this case, the guidewire is disposed inside the array of transducers avoiding the guidewire artifact. However, the selected image presents a shadow artifact which is filtered with the inpainting algorithm (Figure 7(b)). Figure 7(c) illustrates the segmentation result over the unprocessed image, in which the active contour can not cope with the shadow artifact. Figure 7(d) displays the resulting segmentation without interference of the artifact.

Figure 8, corresponding to Set B, illustrates the improvement of the segmentation in the presence of a bifurcation. The inpainting fills the sector where the bifurcation produces a missing region in the image (Figure 8(b)). It can be seen in Figure 8(c) how the external forces try to inflate the curve in this section of the image, and its counteraction with the internal forces. Even

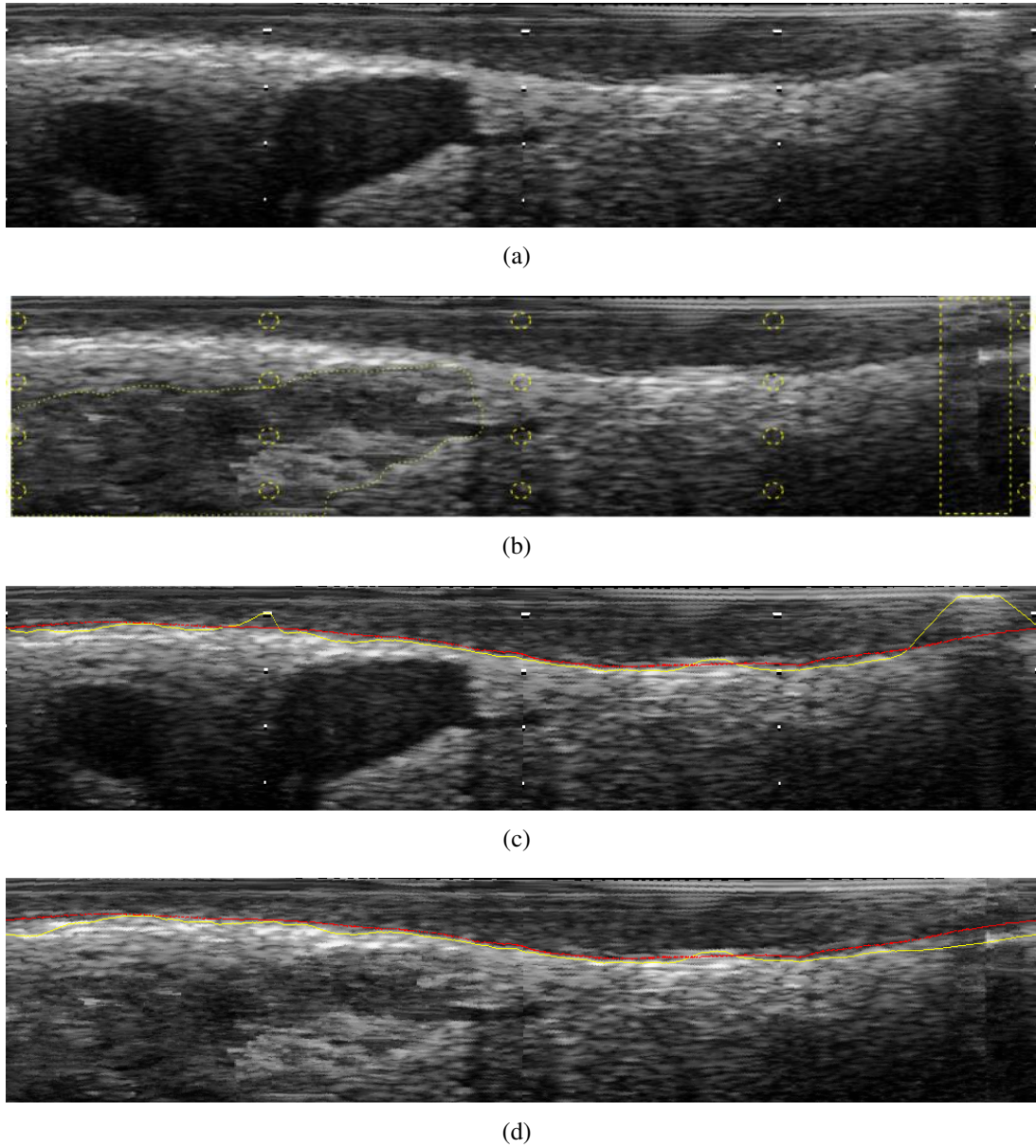
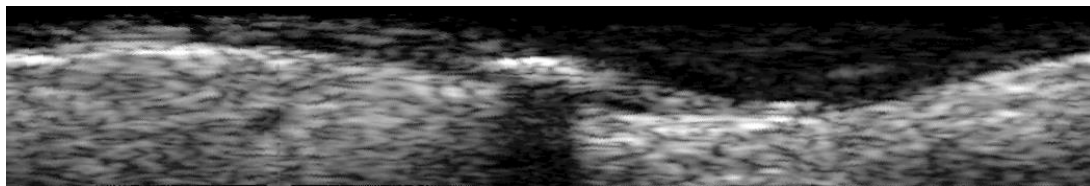
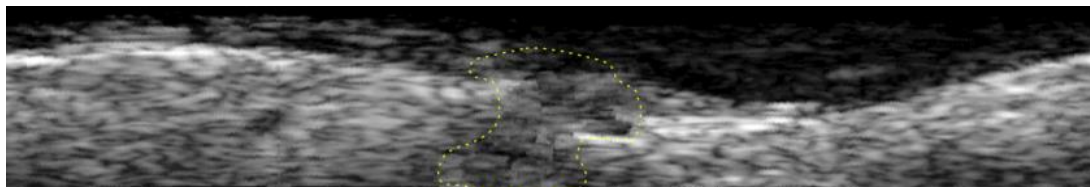


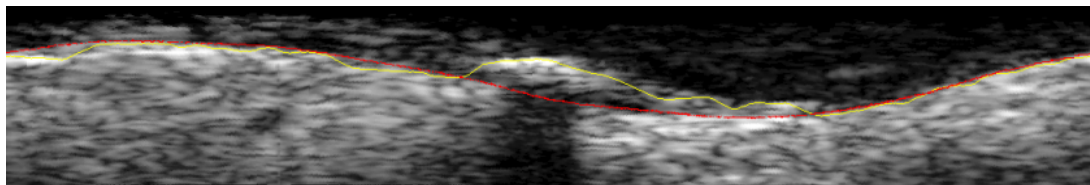
Figure 6: (a) Original image (b) Inpainted image (artifacts marked in yellow dashed line) (c) Original image segmentation (automatic segmentation in solid yellow line, specialist segmentation in solid red line) (d) Inpainted image segmentation



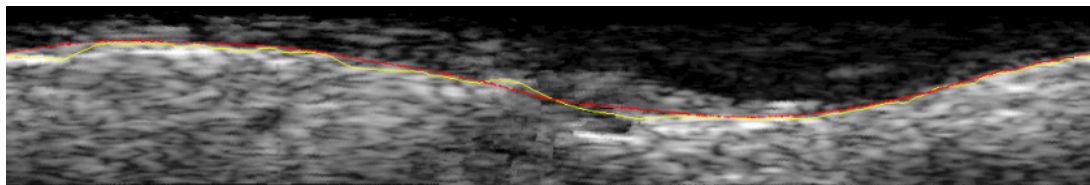
(a)



(b)



(c)



(d)

Figure 7: (a) Original image (b) Inpainted image (artifacts marked in yellow dashed line) (c) Original image segmentation (automatic segmentation marked in solid yellow line, specialist segmentation marked in solid red line) (d) Inpainted image segmentation

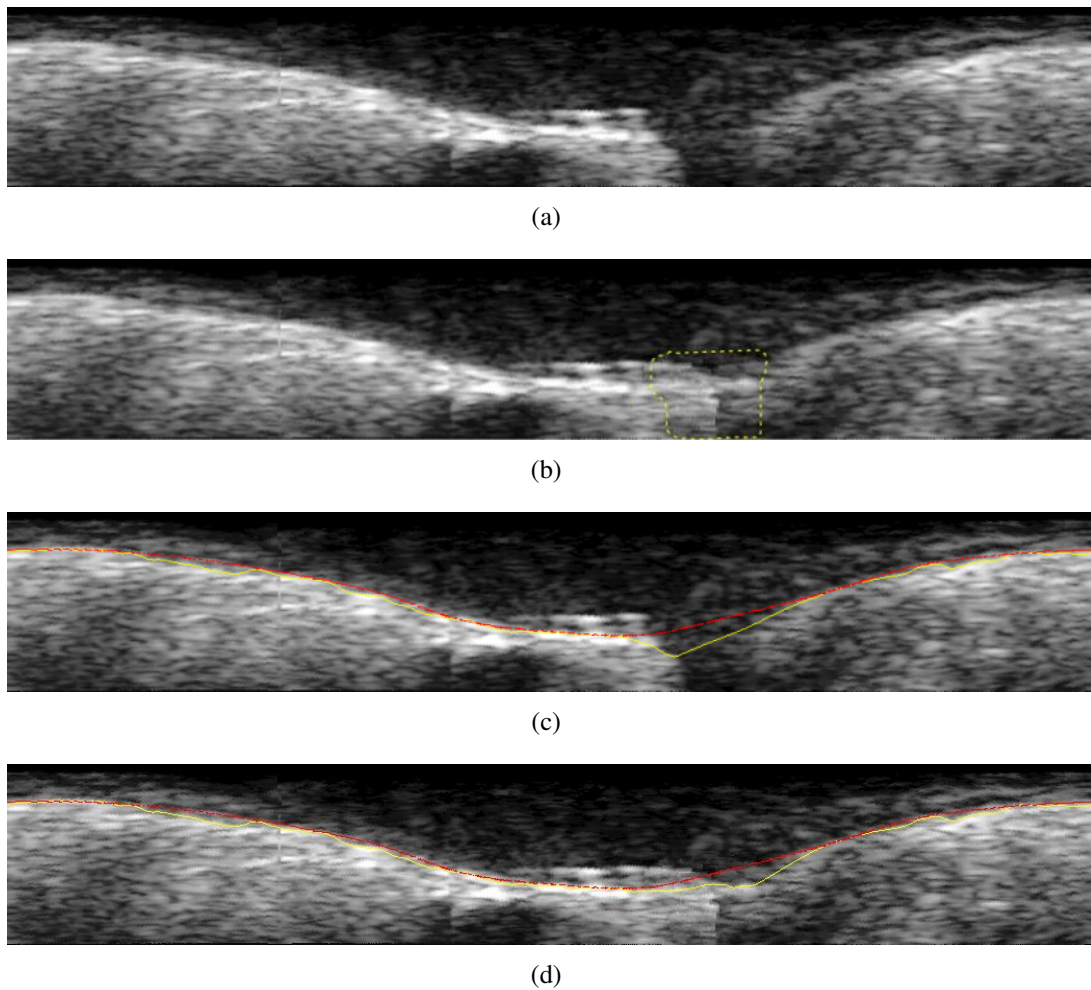


Figure 8: (a) Original image (b) Inpainted image (artifacts marked in yellow dashed line) (c) Original image segmentation (automatic segmentation marked in solid yellow line, specialist segmentation marked in solid red line) (d) Inpainted image segmentation

when the improvement in the segmentation result is not considerable in this case, Figure 8(d) shows a smoother transition, produced by the the inpainting process. The filled area stops the evolution of the active contour.

## 6 DISCUSSION AND CONCLUSIONS

An inpainting method for IVUS segmentation improvement has been presented. The method have been applied in the region where IVUS artifacts are presented. Finally, the resulting image has been tested using a particular segmentation algorithm.

In the field of photography or cinema, it is sufficient that the result of the inpainting procedure be visually plausible whereas in medical imaging this is not enough. Considering that it is difficult to know with certainty what really was the corrupted or missing region, there is a limitation concerning the application of this technique, especially when the resulting image is used for diagnosis. In this work, as there is not a specific medical validation, the result of this restoration was used for improving segmentation and simulation.

The inpainting method proved to be effective erasing white dots, replacing them not arbitrarily as in Balocco et al. (2014). In our case, the inpainting process searches for the best patch that

ensures continuity of the corresponding object boundaries without losing texture information. The method also showed a good performance removing undesired shadows. In any case there is a smooth continuation of the boundaries and a coherent texture filling. Finally, the inpainting performs well to fill with a coherent texture the region marked as side vessel.

It was shown that white dots and shadows interfere with the evolution of a snake-based method as described by Balocco et al. (2014). The removal of white dots and shadow artifact had a positive effect for the segmentation algorithm applied.

Another issue to analyse is the performance of the active contours when bifurcations occur. In these situations, the external forces compete with the internal forces to decide whether to incorporate or not the sector as part of the artery. However, when applying the inpainting method in the bifurcation, the segmentation becomes more similar to the ground truth.

## 7 ACKNOWLEDGEMENTS

The present work has been partially funded by the National Agency for Science and Technology Promotion (ANPCyT, within the project PICT 2010-1287).

## REFERENCES

- Abbott J. and Thurstone F. Acoustic speckle: Theory and experimental analysis. *Ultrasonic Imaging*, 1(4):303–324, 1979.
- Alberti M., Balocco S., Gatta C., Ciompi F., Pujol O., Silva J., Carrillo X., and Radeva P. Automatic bifurcation detection in coronary ivus sequences. *Biomedical Engineering, IEEE Transactions on*, 59(4):1022–1031, 2012. ISSN 0018-9294.
- Balocco S., Gatta C., Ciompi F., Wahle A., Radeva P., Carlier S., Unal G., Sanidas E., Mauri J., Carillo X., Kovarnik T., Wang C.W., Chen H.C., Exarchos T.P., Fotiadis D.I., Destrempe F., Cloutier G., Pujol O., Alberti M., Mendizabal-Ruiz E.G., Rivera M., Aksoy T., Downe R.W., and Kakadiaris I.A. Standardized evaluation methodology and reference database for evaluating ivus image segmentation. *Computerized Medical Imaging and Graphics*, 38(2):70 – 90, 2014. ISSN 0895-6111.
- Bertalmio M., Sapiro G., Caselles V., and Ballester C. Image inpainting. *Proceedings of the 27th Annual Conference on Computer Graphics and Interactive Techniques*, pages 417–424, 2000.
- Bornard R., Lecan E., Laborelli L., and Chenot J.H. Missing data correction in still images and image sequences. *Proceedings of the Tenth ACM International Conference on Multimedia*, pages 355–361, 2002.
- Efros A. and Leung T. Texture synthesis by non-parametric sampling. *Proceedings of IEEE International Conference on Computer Vision*, 2:1033–1038, 1999.
- Haralick R., Shanmugam K., and Dinstein I. Textural features for image classification. *Systems, Man and Cybernetics, IEEE Transactions on*, (6):610–621, 1973.
- Kass M., Witkin A., and Terzopoulos D. Snakes: Active contour models. *International Journal of Computer Vision*, 1(4):321–331, 1988. ISSN 0920-5691.
- Katouzian A., Angelini E., Carlier S., Suri J., Navab N., and Laine A. A state-of-the-art review on segmentation algorithms in intravascular ultrasound (ivus) images. *Information Technology in Biomedicine, IEEE Transactions on*, 16(5):823–834, 2012. ISSN 1089-7771. doi: 10.1109/TITB.2012.2189408.
- Lo Vercio L., del Fresno M., and Vénere M. Segmentación automática de imágenes ivus basada

- en indicadores de textura y modelos deformables. *Mecánica Computacional*, XXXII:3823 – 3834, 2013. ISSN 1666-6070.
- Loizou C. and Pattichis C. *Despeckle Filtering Algorithms and Software for Ultrasound Imaging*. Morgan and Claypool, 2008. ISBN 9781598296211.
- Manterola H. and del Fresno M. Inpainting digital aplicado a la reconstrucción de imágenes de ultrasonido. *Mecánica Computacional*, XXXII(2):3835–3848, 2013. ISSN 1666-6070.
- McInerney T. and Terzopoulos D. Deformable models in medical image analysis: a survey. *Medical image analysis*, 1(2):91–108, 1996.
- McInerney T. and Terzopoulos D. T-snakes: Topology adaptive snakes. *Medical Image Analysis*, 4(2):73 – 91, 2000. ISSN 1361-8415.
- Molinari F., Zeng G., and Suri J. A state of the art review on intima-media thickness (imt) measurement and wall segmentation techniques for carotid ultrasound. *Computer methods and programs in biomedicine*, 100(3):201–221, 2010.
- Perona P. and Malik J. Scale-space and edge detection using anisotropic diffusion. *Pattern Analysis and Machine Intelligence, IEEE Transactions on*, 12(7):629–639, 1990. ISSN 0162-8828. doi:10.1109/34.56205.
- Taki A., Najafi Z., Roodaki A., Setarehdan S., Zoroofi R., Konig A., and Navab N. Automatic segmentation of calcified plaques and vessel borders in ivus images. *International Journal of Computer Assisted Radiology and Surgery*, 3(3-4):347–354, 2008. ISSN 1861-6410. doi: 10.1007/s11548-008-0235-4.